Fabrication of electrospun thermoplastic polyurethane blended poly (l-lactide-co-e-caprolactone) microyarn scaffolds for engineering of female pelvic-floor tissue



2015 Biomed. Mater. 10 015005

(http://iopscience.iop.org/1748-605X/10/1/015005)

Biomedical Materials

PAPER

# Fabrication of electrospun thermoplastic polyurethane blended poly (l-lactide-co-e-caprolactone) microyarn scaffolds for engineering of female pelvic-floor tissue

RECEIVED
11 August 2014

REVISED
8 November 2014

ACCEPTED FOR PUBLICATION
11 November 2014

PUBLISHED
29 December 2014

Min Hou[1], Qingkai Wu[1,4], Miao Dai[1], Peirong Xu[1], Chaochen Gu[2], Xiang Jia[1], Jie Feng[1] and Xiumei Mo[3]

[1] Department of Obstetrics And Gynecology, Shanghai Jiao Tong University Affiliated Sixth People's Hospital, No 600 Yi Shan Road, Shanghai 200233, People's Republic of China
[2] School of Mechanical Engineering, Shanghai Jiao Tong University, No 800 Dong Chuan Road, Shanghai 200240, People's Republic of China
[3] College of Chemistry and Chemical Engineering and Biological Engineering, Donghua University, 2999 Ren Min Road, Shanghai, 201620, People's Republic of China
[4] Author to whom correspondence should be addressed.

**E-mail:** wuqingkai@sjtu.edu.cn, med@dhu.edu.cn

**Keywords:** electrospinning, 3D scaffold, microyarn, cell infiltration, pelvic tissue

## Abstract

Potential scaffolds for repair of the female pelvic floor require new materials and fabrication by novel methods to improve cellular infiltration. An 'ideal' engineered scaffold for pelvic-floor tissue should mimic the three-dimensional (3D) network of the extracellular matrix (ECM), which possesses intricate macro- and nano-architecture. In this study, a series of blended poly(l-lactide-co-ecaprolactone) P(LLA-CL)/thermoplastic polyurethane (TPU) microyarn/microfibrous scaffolds were produced with different weight ratios via dynamic liquid electrospinning and electrospinning. Both biopolymers were dissolved in 1,1,1,3,3,3-hexafluoro-2-propanol (HFIP). Our data showed the mean diameter of microyarn scaffolds to be significantly larger than that of microfibers. Microyarn scaffolds possessed large pore sizes and high porosity. There was no significant difference between the mechanical properties of microyarn and microfibrous scaffolds. Fourier-transform infrared spectroscopy suggested that intermolecular bonds were not present between the molecules of TPU and P(LLA-CL). Morphologic observations using scanning electron microscopy and inverted fluorescence microscopy showed that adipose-derived stem cells labeled with enhanced green fluorescent protein could grow well along or within blend microyarns and migrate within the novel 3D scaffolds. Hematoxylin and eosin staining demonstrated that cell infiltration on microyarn scaffolds was significantly enhanced. The CCK-8 assay showed that microyarns could significantly facilitate cell proliferation compared with microfibrous scaffolds. These results suggested that blend microyarns of P(LLA-CL)/TPU designed to mimic the ECM for female pelvic-floor tissue may be excellent macroporous scaffolds for tissue repair.

## 1. Introduction

Dysfunction of the pelvic floor means that the pelvic floor cannot support the pelvic organs and/or cannot allow these organs to function normally [1]. To improve quality of life, many women suffering from pelvic-floor dysfunction require surgical intervention, but the prevalence of success of surgery is low and recurrence is common [2]. Therefore, to improve the outcome of conventional surgery for pelvic-floor dysfunction, numerous biological and synthetic graft materials (i.e. meshes, slings) have been used in pelvic reconstructive surgery. Such materials have important roles in reinforcement of weak or defective supportive tissues, substitution of absent supportive tissue, induction of new supportive tissue and consolidation to complement conventional surgical methods [3].

Synthetic materials (absorbable or non-absorbable) used in reconstructive surgery of the pelvic floor can be classified broadly into macroporous materials (e.g. polypropylene mesh), microporous materials (e.g. polytetrafluoroethylene mesh) and macroporous mesh with multifilamentous or microporous components (e.g. polyester–silicone-coated mesh, which is rarely used in pelvic reconstructive surgery) [4, 5]. For these synthetic materials, complications include infection,

erosion, dyspareunia, voiding difficulties and wound granulation [6].

The 'ideal' graft would be physically and chemically inert, readily available, non-carcinogenic, mechanically strong, not physically modified by body tissue, inexpensive and carry a minimal risk of rejection and infection of tissue [7]. Towards this goal, searching for a material that is non-toxic, resistant to infection, inexpensive and macroporous with a moderate rate of degradation and with mechanical properties that match those of pelvic tissue is imperative.

Conventional fibrous scaffolds fabricated by electrospinning can mimic the length of natural extracellular matrix (ECM) [8], and are used widely in various types of tissue engineering. However, conventional electrospun fibrous scaffolds provide only a superficial porous structure comprised entirely of tightly packed nanofiber layers, which reduces pore size and limits cellular ingress [9]. Therefore, it is necessary to develop novel technology that can be used to fabricate electrospun scaffolds with stable three-dimensional (3D) structures, more interconnected macropores, higher porosity and enhanced cellular infiltration. Such a scaffold would better mimic native ECM in terms of structure or function.

To solve this problem, numerous methods for improving cellular ingress have been used. Van Tienen *et al* developed a method that improved infiltration by increasing porosity. They obtained an optimal pore size for cell infiltration using porous foams and sponges with a low compression modulus and sufficient diameter between macropores [10]. Another study produced dual-polymer composite fiber-aligned scaffolds by co-electrospinning poly(3-caprolactone) and poly(ethylene oxide) with removal of the poly(ethylene oxide) component after seeding mesenchymal stem cells on aligned scaffolds for three weeks to improve pore size and cell infiltration [11]. However, cell ingrowth into these dense structures was slow and the mechanical properties of these scaffolds variable. Another strategy is to embed the hydrogel into a scaffold using a simultaneous electrospraying–electrospinning setup [12]. This method improves cell infiltration, but the pockets of this scaffold do not interconnect with each other so the cells are unlikely to grow throughout the scaffold in a consistent manner. Another approach involves increasing the pore size; fibers are obtained using an earthed rotating aluminum mandrel that can twist fiber-to-fiber bundles. However, nanofibers are collected as dense structures [13].

Based on the research mentioned above, we adopted dynamic liquid electrospinning technology to fabricate 3D blended poly(l-lactide-co-ecaprolactone) P(LLA-CL)/thermoplastic polyurethane (TPU) microyarn scaffolds to improve their pore size and aid cell infiltration. The dynamic liquid electrospinning setup comprised a high-voltage power supply, microsyringe pump, a rotating mandrel collector and a water bath (to remove microfibers).

These microyarn scaffolds are conducive to cell penetration because they maintain a porous microstructure after freeze drying [14]. P(LLA-CL) was chosen as one of the raw materials of this scaffold due to its lack of toxicity and degradability as well as its high biocompatibility [15]. TPU was chosen as the other raw material due to its excellent mechanical properties and high biocompatibility and susceptibility to degradation, which enables its use in the engineering of vessels, catheters and prosthetic heart valves [16, 17]. Surface morphology of scaffolds was characterized by scanning electron microscopy (SEM). ImageJ software (National Institutes of Health, Bethesda, MD, USA) was used to measure fiber diameters. The chemical composition of electrospun P(LLA-CL)/TPU blended microyarn scaffolds was verified by Fourier-transform infrared (FTIR) spectroscopy. The mechanical behavior of microyarn scaffolds was measured by means of tensile tests. Using cultures of rabbit adipose-derived stem cells (ADSCs), the attachment, proliferation and infiltration of cells on scaffolds were investigated by Cell Count Kit-8 (CCK-8) assay and hematoxylin and eosin (H & E) staining.

## 2. Materials and methods

### 2.1. Materials

P(LLA-CL) (LA:CL = 75:25; molecular weight = 340 000) was purchased from Daigang Bio-Tech Co., Ltd (Jinan, China). TPU was obtained from Austin Novel Materials Co., Ltd (Zhang Jiagang, China). 1,1,1,3,3,3-Hexafluoro-2-propanol (HFIP) (used for dissolving P(LLA-CL) and TPU) was provided by Da-Rui Co., Ltd (Beijing, China). Dulbecco's modified Eagle's medium (DMEM) and other cell-culture reagents were bought from Sigma–Aldrich Chemical Co., Ltd (Saint Louis, MO, USA). Lentivirus was purchased from Jikai Chemical Technology Co., Ltd (Shanghai, China). CCK-8 was obtained from Dojindo Laboratories (Tokyo, Japan).

### 2.2. Scaffold fabrication

*2.2.1. Electrospinning of conventional electrospun scaffolds.*

A series of P(LLA-CL)/TPU solutions for electrospinning were prepared by dissolving P(LLA-CL) and TPU blended in HFIP with different weight ratios of P(LLA-CL) to TPU (100:0, 75:25, 50:50, 25:75, 0:100) at 8% (*w/v*) respectively. Conventional electrospun scaffolds were produced using a setup comprising a high-voltage power supply (BGG6-358; Bmeico, Beijing, China), syringe pump (789100C; Cole-Parmer, Vernon Hills, IL, USA) and an earthed collection system (a solid plate). Prepared pure solutions and polymer solutions were fed from a 5 mL or 10 mL plastic syringe to a blunt-ended needle connected to a high-voltage power supply at 0.8–1.5 mL $h^{-1}$. The electrospinning voltage was 12–17 kV. The distance between the fiber collector and needle tip was 12–16 cm. All experiments were undertaken at room temperature (15–30 °C).

Subsequently, all electrospun fibers were vacuum dried for 48 h at room temperature and stored in desiccators. For all experiments, microfibrous scaffolds were vacuum dried at room temperature for 24 h to remove residual solvent and stored in a vacuum-dry oven.

*2.2.2. Electrospinning of microyarn scaffolds.*
In contrast with conventional electrospinning, we fabricated microyarn scaffolds using a dynamic liquid electrospinning setup as described above. A water bath was placed between the needle tip and rotating mandrel collector. In the middle of the bottom of the water bath was a hole (diameter 8 mm) that allowed water to flow as a water vortex. Microfibers were deposited on the water surface due to eddy currents. Microfibers were twisted into fiber bundles and collected on the rotating mandrel (60 rpm). All other experimental processes and parameters were identical to those for electrospinning of conventional electrospun scaffolds. Finally, microyarn scaffolds were frozen at –80 °C for 2 h, freeze dried for 24 h and stored in a vacuum-dry oven.

### 2.3. Scaffold characterization

*2.3.1. SEM.*
Dry microfibrous scaffolds and microyarn scaffolds were sputter-coated with gold for 40 s at 4 MA. Morphology was imaged using a Scanning Electron Microscope (TM-100; Hitachi, Tokyo, Japan) at an acceleration voltage of 10 kV. Mean diameters were measured on the basis of SEM images using ImageJ v1.47 (NIH) using 100 randomly selected fibers. Pore sizes were determined from ≥100 pores in the SEM images.

*2.3.2. Porosity of electrospun scaffolds.*
The thickness of electrospun microfibrous and microyarn scaffolds of P(LLA-CL)/TPU with different ratios at 8% (*w/v*) was measured with a Micrometer (Measuring and Cutting Tools Co., Ltd, Shanghai, China). The apparent density and porosity of scaffolds were calculated according to the following equations [18]:

$$\text{Apparent density (g/cm}^3\text{)} = \frac{\text{Mass(mg)} \times 10}{\text{thickness}(\mu\text{m}) \times \text{area(cm}^2\text{)}}$$

$$\text{Porosity} = \left(1 - \frac{\text{apparent density(g/cm}^3\text{)}}{\text{bulk density of raw material(g/cm}^3\text{)}}\right) \times 100\%$$

### 2.4. Mechanical testing

Tensile tests were conducted using a Universal Materials Tensile Tester (H5K-S Hounsfield; Tinius Olsen, Inc., Horsham, PA, USA) with a 50 N load cell and a 30 mm gauge length at a uniform speed of 10 mm $min^{-1}$. Each scaffold was cut into five strips (length 50 mm; width 10 mm) for mechanical testing. Before the stress–strain test, strips were pre-processed in an incubator with phosphate-buffered saline (PBS) at 37 °C overnight. The ultimate tensional strength and percentage elongation were calculated from five independent samples obtained from microfibrous and microyarn scaffolds. The largest stress was used as a measure of strength; elongation was calculated using the elongated length/original length. Real areas of samples changed constantly with elongation of the samples. Hence, it was difficult to obtain the real areas, so original areas were used to calculate stresses. Then, the stress was calculated using the tensile force/original area.

### 2.5. FTIR spectroscopy

The chemical composition of P(LLA-CL) blended TPU microyarn scaffolds at different weight ratios was analyzed and characterized by FTIR spectroscopy. The wavelength range in absorption mode was 2000–800 $cm^{-1.}$

### 2.6. Isolation, culture and transfection of cells

ADSCs were harvested from the adipose tissues of the groins of two New Zealand white rabbits. We minced and digested adipose tissue with 0.15% (*w/v*) type-I collagenase and centrifuged the mixture as previously described [19]. Deposits containing ADSCs were resuspended and cultured in DMEM (Gibco, Billings, MT, USA) with 10% fetal bovine serum (Invitrogen, Carlsbad, CA, USA), 1% penicillin and streptomycin (Yuanye Biological Technology Co., Ltd, Beijing, China) on a 10 cm petri dish in a 37 °C incubator with 5% $CO_2$ in the air. When ADSCs reached 90% confluence, they were detached from the petri dish by digestion with 0.25% trypsin and passaged. When the density of cells in the culture flask reached $10^5$ $mL^{-1}$, ADSCs were transfected with lentivirus-containing enhanced green fluorescent protein (EGFP) at passage-4 according to manufacturer instructions (Jikai Genechem Co., Ltd, Shanghai, China). Transfected ADSCs continued to culture in a 5% $CO_2$ incubator at 37 °C. Cells at passage-5 were used.

Two groups of scaffolds were cut into small samples (length 10 mm; width 10 mm) and placed in 24-well tissue culture plates (Costar®; Corning, Corning, NY, USA). Plates were sterilized by processing with 75% ethanol and ultraviolet light for 2 h. Next, we immersed these sterilized samples into the culture medium for 4 h and then transplanted labeled EGFP ADSCs onto the sterilized scaffolds for 4 h ($0.5 \times 10^4$/sample; cells cultured in a 5% $CO_2$ incubator at 37 °C). Finally, we added the culture medium to each well. We changed the culture medium every two days.

### 2.7. Adhesion and proliferation of cells

Microfibrous and microyarn scaffolds were cut into 0.5 cm × 0.5 cm squares. The method of sterilization was as described above. After washing thrice with sterile PBS, small scaffolds were placed in 96-well culture

**Table 1.** Microfiber diameter, tensile strength and elongation at break, porosity and pore size of different electrospun mats ($n = 5$) (mean ± SD).

| 8% P(LLA-CL)/ TPU weight ratio | Specimen thickness (mm) | Fiber diameter ($\mu$m) | Tensile strength (Mpa) | Ultimate strain (%) | Porosity (%) | Pore size ($\mu m^2$) |
|---|---|---|---|---|---|---|
| 100:0 | 0.09 ± 0.01 | 0.83 ± 0.19 | 6.70 ± 0.53 | 83.2 ± 10.28 | 69.64 ± 1.56 | 68.30 ± 36.24 |
| 75:25 | 0.10 ± 0.02 | 1.12 ± 0.16 | 7.51 ± 0.76 | 116.3 ± 15.24 | 67.24 ± 2.10 | 82.3 ± 40.55 |
| 50:50 | 0.11 ± 0.02 | 1.20 ± 0.20 | 10.64 ± 1.29 | 123.46 ± 7.89 | 63.12 ± 1.78 | 72.51 ± 43.21 |
| 25:75 | 0.10 ± 0.01 | 1.25 ± 0.39 | 13.92 ± 1.23 | 144.67 ± 12.11 | 57.65 ± 2.12 | 64.4 ± 39.56 |
| 0:100 | 0.11 ± 0.01 | 1.26 ± 0.43 | 17.48 ± 3.47 | 156.30 ± 13.57 | 51.52 ± 1.13 | 57.76 ± 24.8 |

**Table 2.** Microyarn diameter, tensile strength and elongation at break, porosity and pore size of different electrospun scaffolds ($n = 5$) (mean ± SD).

| 8% P(LLA-CL)/ TPU weight ratio | Specimen thickness (mm) | Fiber diameter ($\mu$m) | Tensile strength (Mpa) | Ultimate strain (%) | Porosity (%) | Pore size ($\mu m^2$) |
|---|---|---|---|---|---|---|
| 100:0 | 0.14 ± 0.02 | 15.44 ± 4.21 | 5.73 ± 0.76 | 75.00 ± 8.56 | 81.89 ± 3.98 | 576.86 ± 396.58 |
| 75:25 | 0.16 ± 0.01 | 12.25 ± 2.63 | 7.29 ± 1.87 | 145.80 ± 14.52 | 76.89 ± 3.04 | 501.46 ± 402.44 |
| 50:50 | 0.14 ± 0.05 | 16.07 ± 6.04 | 11.5 ± 3.43 | 164.34 ± 12.56 | 80.45 ± 3.62 | 587 ± 348.79 |
| 25:75 | 0.14 ± 0.03 | 15.38 ± 4.24 | 7.69 ± 2.04 | 161.30 ± 14.36 | 77.65 ± 2.97 | 565.42 ± 256.25 |
| 0:100 | 0.14 ± 0.03 | 11.14 ± 3.48 | 4.27 ± 1.23 | 177.93 ± 16.78 | 78.59 ± 3.32 | 524 ± 204.56 |

plates and immersed in culture medium for 2 h in a 5% $CO_2$ incubator at 37 °C. ADSCs were seeded on these small scaffolds and in 96-well culture plates (controls) at $10^4$ cells/well and incubated under the conditions described above.

For cell-adhesion tests, assays were carried out 4 h after cell seeding. Cell proliferation on scaffolds was investigated through CCK-8 assays for 1, 4 and 7 d. At each time point, the complete medium was replaced with fresh total medium containing 10% CCK-8 reagent as per manufacturer instructions. After 2–4 h of incubation, absorbance values for all samples were simultaneously measured at 450 nm using a Microplate Reader (550; Bio-Rad, Hercules, CA, USA). Each experiment was evaluated from the three samples.

### 2.8. Cell morphologies on scaffolds imaged by SEM and inverted fluorescence microscopy

Transfected ADSCs seeded on scaffolds were viewed using an Inverted Fluorescence Microscope (DMIL (Leica, Wetzlar, Germany) with a 50 W X-Cite® Lamp (EFOS, New York, NY, USA) after 24 h with an excitation filter of 460–550 nm. After ADSCs had been seeded on samples of microfibrous and microyarn scaffolds for 1, 4 and 7 d, they were fixed in 2.5% glutaraldehyde at 4 °C overnight, soaked in 1% osmium tetroxide for 1 h and rinsed thoroughly thrice with PBS. Samples were dehydrated in a graded series of ethanol solutions (30%, 50%, 70%, 80%, 90%, 100%), freeze dried for 24 h, sputter-coated with gold and then observed/imaged using the scanning electron microscope.

### 2.9. Histological analyses

Cell ingrowth into scaffolds was assessed by H&E staining at 1, 4 and 7 d. We washed samples thrice with PBS and fixed them in 4% paraformaldehyde overnight. Samples were dehydrated, embedded in paraffin blocks and then made into paraffin sections. H&E staining was carried out and cell infiltration observed/imaged under a light microscope.

### 2.10. Statistical analyses

Quantitative data were analyzed using SPSS v19.0 (IBM, Armonk, NY, USA) and expressed as the mean ± standard deviation (SD). Statistical differences among groups were determined by one-way ANOVA. $p < 0.05$ was considered significant.

## 3. Results

### 3.1. Morphology of TPU/P(LLA-CL)-blended microfibrous and microyarn scaffolds

TPU and P(LLA-CL) at all weight ratios were fabricated to interconnected networks and microyarns with randomly oriented fibers and fiber bundles. Morphologies of the series of electrospun microfibrous and microyarn scaffolds mimicked the ECM closely (figures 2(*b*)–(*j*)). SEM images revealed that several microfibers were twisted into microyarns. There was no difference in the structure of scaffolds among the different weight ratios tested. Therefore, the weight ratios of both polymers did not have an effect on morphology. The diameter distribution of microfibers and microyarns at blend ratios from 100:0 to 0:100 are shown in tables 1 and 2.

### 3.2. Mechanical testing

The tensile stress–strain curves of P(LLA-CL)/TPU-blended microfibrous and microyarn scaffolds are shown in figure 3 and tables 1 and 2. Mean tensile strength and elongation at break of microfibrous scaffolds increased gradually and significantly with an

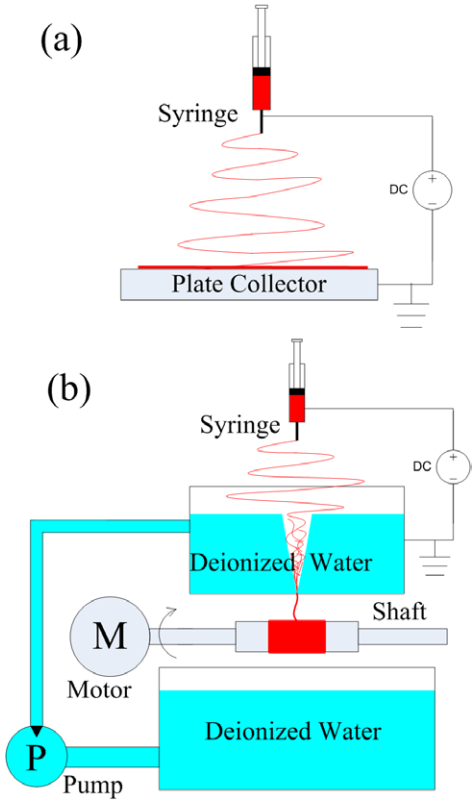


**Figure 1.** Schematic of a coventional electrospinning system (*a*) and dynamic liquid electrospinning system (*b*) for fabrication of microfibrous and microyarn scaffolds.

increasing weight ratio of TPU. However, microyarn scaffolds of P(LLA-CL)/TPU with a weight ratio of 50:50 possessed higher tensile strength compared with pure TPU, pure P(LLA-CL) and P(LLA-CL)/TPU at other weight ratios.

### 3.3. Porosity and pore size of electrospun scaffolds

Porosity of microyarn and microyarn scaffolds with different weight ratios of TPU to P(LLA-CL) are shown in tables 1 and 2. Microyarn scaffolds exhibited higher porosity (79.09 ± 3.22% versus 61.8 ± 1.64%) and larger pore size (550.78 ± 142.60 versus 69.05 ± 19.18 $\mu m^2$) compared with microfibrous scaffolds.

### 3.4. FTIR spectroscopy

Figure 4 shows absorption peaks (in $cm^{-1}$) at 3328, 1701 and 1597 that correspond to N-H stretching, C = O stretching and N-H bending in pure TPU, whereas an absorption peak at 1754 corresponds to C = O stretching in pure P(LLA-CL). All peaks were observed in the P(LLA-CL)/TPU FTIR spectrum, suggesting that TPU and P(LLA-CL) were present in P(LLA-CL)/TPU microyarn scaffolds. Comparison of the real spectrum of P(LLA-CL)/TPU with the calculated spectrum of P(LLA-CL)/TPU shows no new peaks and no disappearance of existing peaks, and they are well matched. Hence, it is very unlikely that a chemical reaction occurred between P(LLA-CL) and TPU.

### 3.5. Cell morphologies on scaffolds

Cell morphology and interactions between ADSCs with microfibrous and microyarn scaffolds were evaluated by SEM and inverted fluorescence microscopy (figures 5 and 6). ADSCs interacted and grew well on the surfaces of microyarn and microyarn scaffolds on day 1, and ADSCs on the two scaffolds had fusiform or polygonal shapes (figures 5(*a*) and (*b*) and 6(*b*) and (*c*)). On days 4 and 7, ADSCs were longer on microyarn scaffolds than those on microfibrous scaffolds. Cells seeded on microfibrous scaffolds were randomly distributed. Some cells seeded on microyarn scaffolds were elongated along microyarns, whereas others were randomly distributed between microyarns (figures 5(*c*) and (*d*)). All cell-seeded scaffolds were filled with 'sheets of cells' and possibly ECM secreted by ADSCs (figures 5(*e*) and (*f*)).

### 3.6. Adhesion and proliferation of cells

Adhesion and proliferation of ADSCs on electrospun microfibrous and microyarn scaffolds were assessed by culturing cells on these two types of scaffolds for 7 d (figure 7). Cell adhesion was observed by counting the cells 4 h after seeding. There was no significant difference in cell proliferation between microfibrous and microyarn scaffolds at 1 d and 4 d ($p > 0.05$). However, at 7 d, microyarn scaffolds exhibited significantly higher proliferation than that observed on microfibrous scaffolds ($p < 0.05$).

### 3.7. Histological analyses

H&E-stained images of cell-seeded microyarn and microyarn scaffolds are shown in figure 8. On day 1, day 4 and even on day 7, few ADSCs had migrated to within microfibrous scaffolds (figures 8(*a*), (*c*) and (*e*)). On day 1 and even on day 7, they were limited to the scaffold surface. However, on day 1, cells grew into microyarn scaffolds to a depth of ≈250 $\mu$m. By day 4, cells had infiltrated to a depth of ≈350 $\mu$m (figure 8(*d*)). By day 7, ADSCs had migrated through the entire scaffold to a depth of 450 $\mu$m (figure 8(*f*)).

## 4. Discussion

We focused on 3D blended P(LLA-CL)]/TPU microyarn scaffolds fabricated using novel dynamic liquid electrospinning technology. Microyarn scaffolds can offer sufficiently macroporous structures that possess native characteristics of pelvic tissue. Such characteristics include high porosity, large pore size and suitable mechanical properties for the attachment and infiltration of cells in tissue engineering. These features will help to facilitate nutrient transport and metabolite release as well as to duplicate pelvic tissue in terms of structure and function [20, 21].

Previously, conventional electrospun scaffolds required additional post-fabrication modifications to alter the characteristics and stability of microfibrous scaffolds to increase the cell porosity. TPU has been

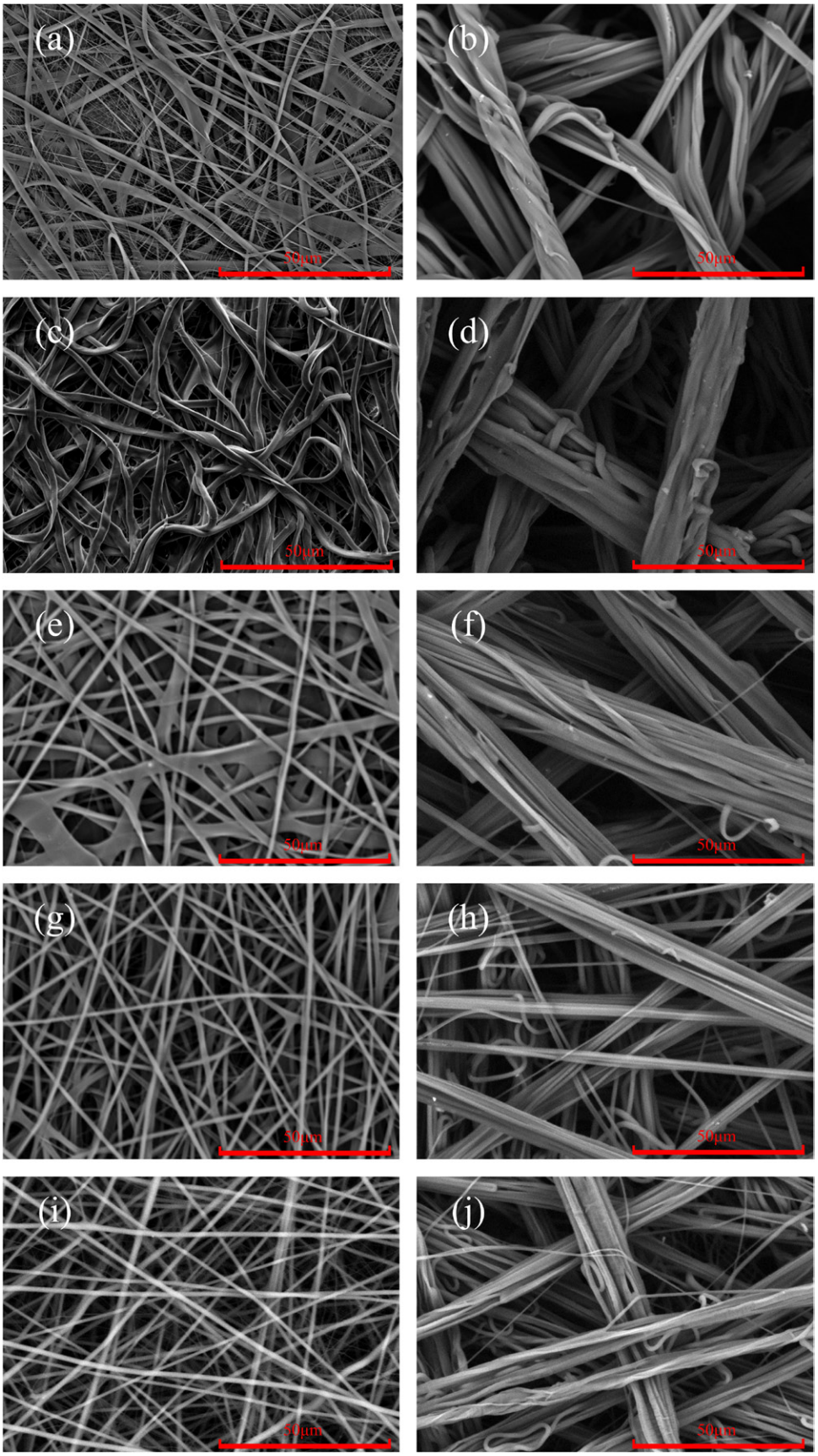


**Figure 2.** SEM images at 8% (*w/v*) with different blend ratios of TPU to P(LLA-CL) microfibers, (*a*) 100:0, (*c*) 75:25, (*e*) 50:50, (*g*) 25:75 and (i) 0:100, and microyarns, (b) 100:0, (*d*) 75:25, (*f*) 50:50, (*h*) 25:75 and (*j*) 0:100.

used for tissue engineering because of its good biocompatibility and excellent mechanical properties [16]. P(LLA-CL) has been employed in tissue engineering due to its excellent elasticity and biodegradability [22]. Therefore, novel scaffolds blended from P(LLA-CL) and TPU were fabricated using dynamic liquid electro-

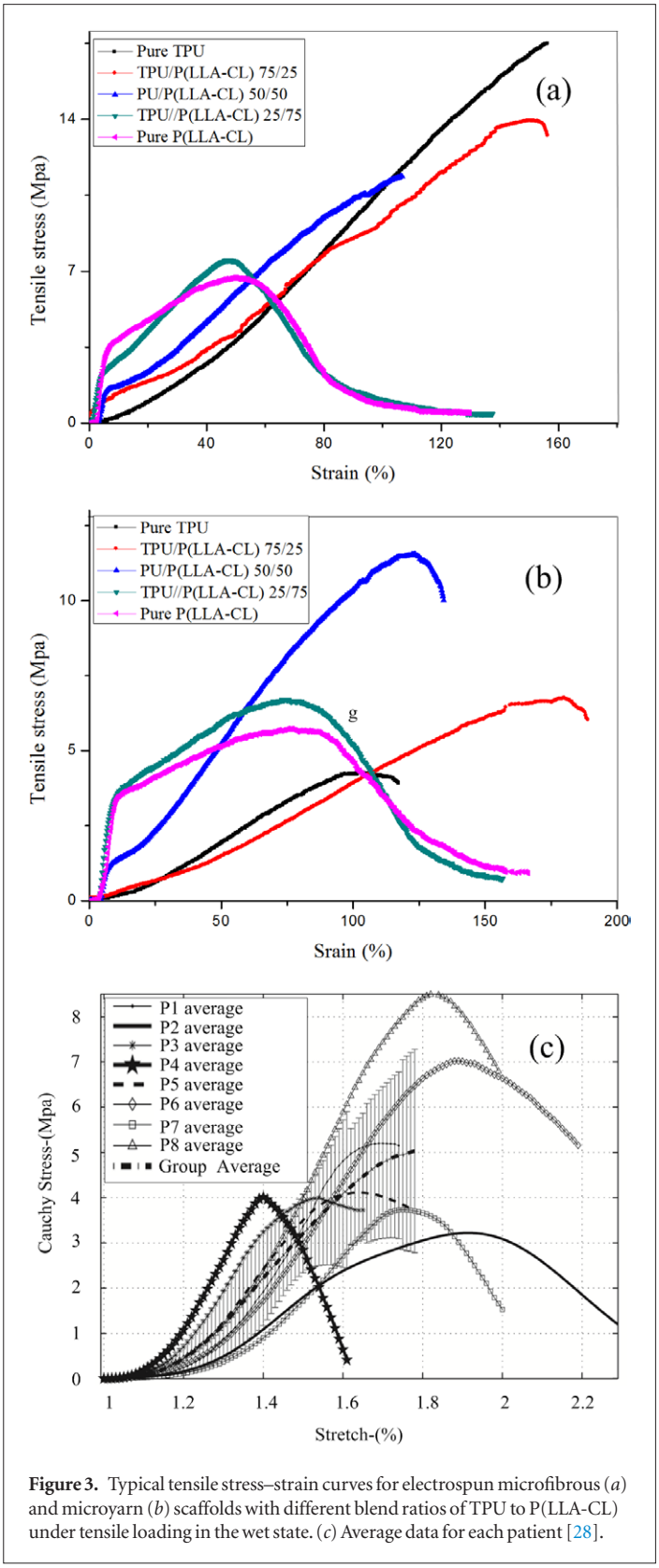


**Figure 3.** Typical tensile stress–strain curves for electrospun microfibrous (*a*) and microyarn (*b*) scaffolds with different blend ratios of TPU to P(LLA-CL) under tensile loading in the wet state. (*c*) Average data for each patient [28].

spinning. These scaffolds had better mechanical properties and improved biocompatibility for engineering of female pelvic tissue.

Selecting a suitable organic solvent is very important for scaffold fabrication. HFIP is an ideal organic solvent because it allows full extension of the polymer and complete evaporation without leaving residues on the formed fibers [23]. We found that TPU and P(LLA-CL) could dissolve in HFIP whether blended together or separately upon electrospinning. Hence, HFIP was selected as the solvent for P(LLA-CL)/TPU blends. TPU and P(LLA-CL) were dissolved in HFIP at different blend weight ratios of P(LLA-CL) to TPU (100:0, 75:25, 50:50, 25:75, 0:100). The concentration of the solution was 8% (*w/v*).

The surface morphology and mean diameter of microfibrous and microyarn scaffolds were ana-

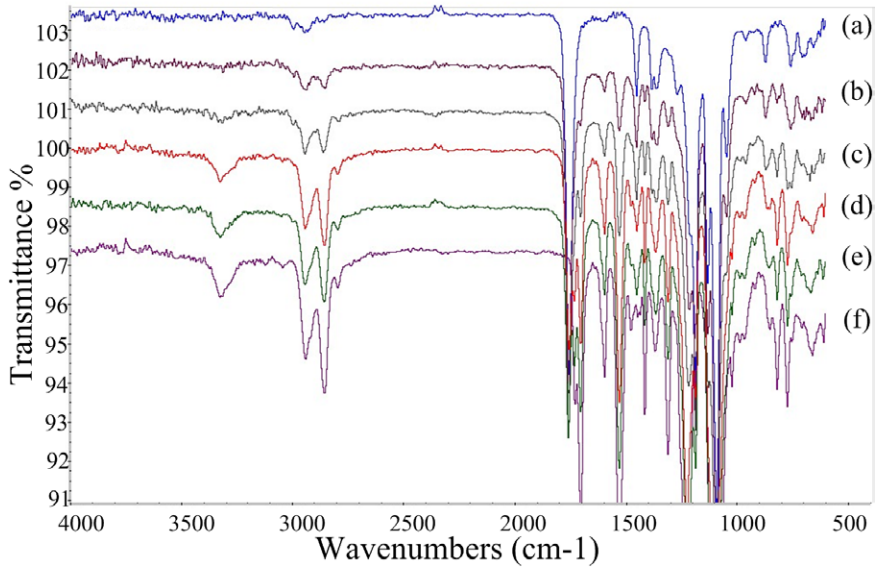


**Figure 4.** FTIR spectra of electrospun P(LLA-CL)/TPU microyarns with different blend ratios of TPU to P(LLA-CL): (*a*) 100:0, (*b*) 75:25, (*c*) calculated P(LLA-CL)/TPU spectrum, (*d*) 50:50, (*e*) 25:75 and (*f*) 0:100.

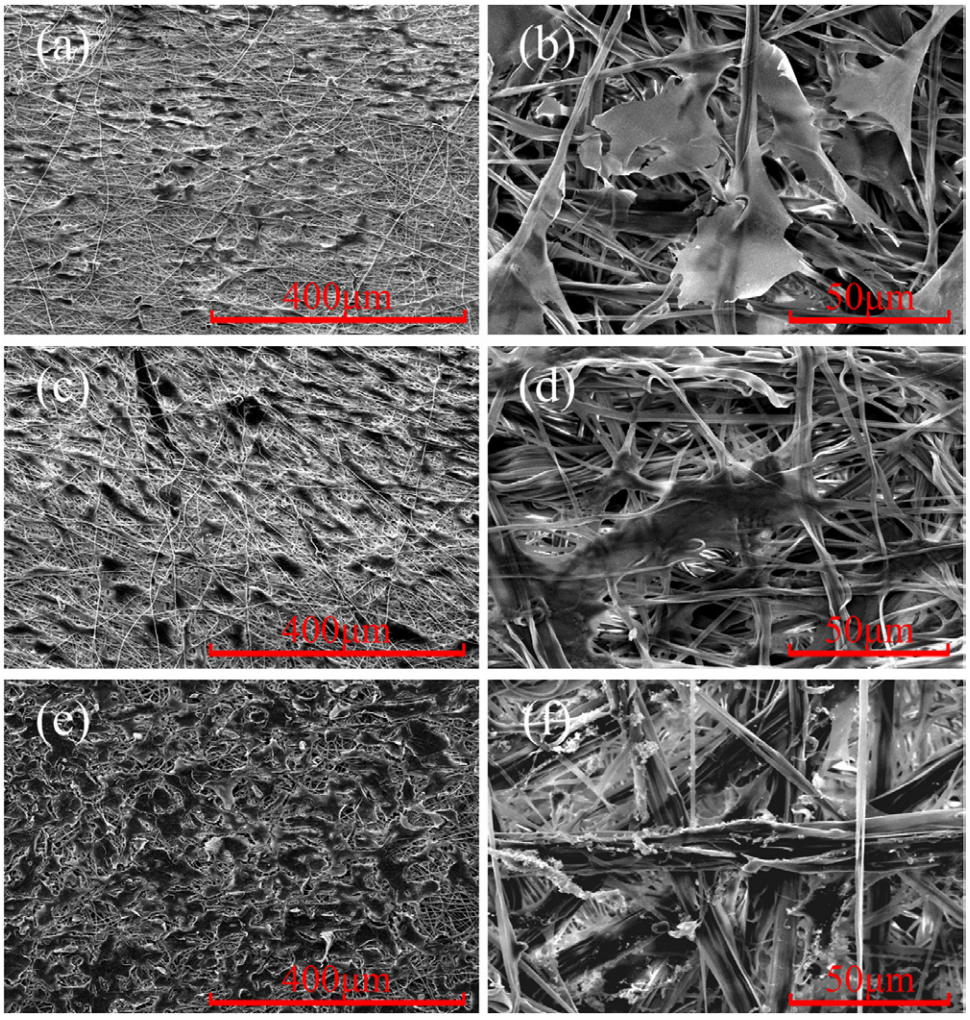


**Figure 5.** SEM images of ADSCs cultured on P(LLA-CL)/TPU microfiber (*a*), (*c*), (*e*), and microyarn (*b*), (*d*), (*f*) scaffolds for 1, 4 and 7 d, respectively.

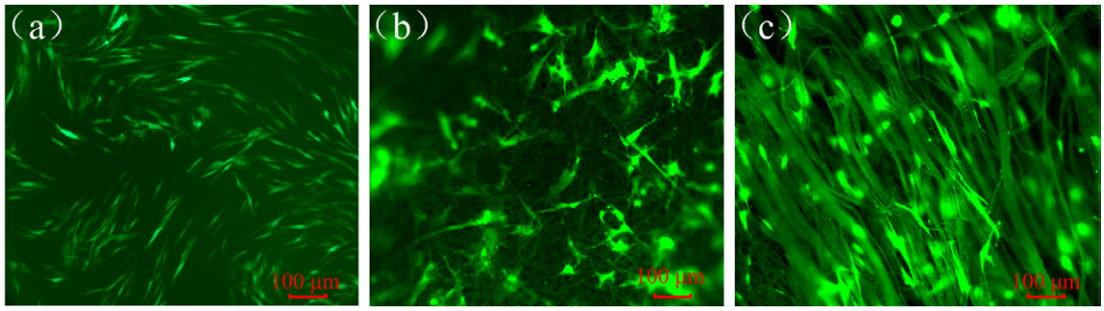


**Figure 6.** Detection of EGFP-labeled ADSCs on day 1 of cell culture, (*a*) TCP, (*b*) P(LLA-CL)/TPU microfibrous and (*c*) microyarn scaffolds, at 50 × magnifications.

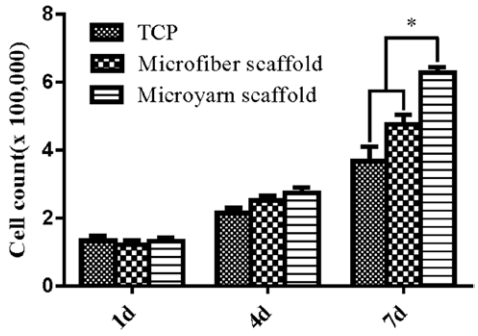


**Figure 7.** Results of CCK-8 assay of ADSCs cultured on TCP, microfibrous scaffolds and microyarn scaffolds for 1, 4 and 7 d. * denotes a significant difference between the two groups ($p < 0.05$).

lyzed using SEM. The mean diameter of microfibers was ≈1.132 ± 0.18 $\mu$m and increased gradually with increasing TPU content in the blend (figure 2, table 1). We have an explanation for this phenomenon. Upon electrospinning, when P(LLA-CL) is added to the blend solution, more ions will be generated and a higher charge density carried compared with pure TPU. Hence, the conductivity of the solution increases, which tends to generate microfibers of a smaller diameter. The mean diameter of microyarns twisted by numerous fibers (figure 2, table 2) was ≈14.05 ± 2.21 $\mu$m and the diameter of microyarns varied between different weight ratios. We have an explanation for this phenomenon. In a dynamic liquid electrospinning system (figure 1), the water vortex is a very important parameter because it can twist electrospun microfibers into microyarns. When microfibers fall upon the water surface, they flow with the water vortex under eddy currents and eventually form microyarns, which are collected by the rotating mandrel [24]. However, when TPU falls on the water surface, fibers cannot readily flow with the water vortex under eddy currents because of the poor hydrophilicity of TPU *in vitro*. Nevertheless, most microyarn scaffolds formed 3D macropores, and the structure of microyarn scaffolds was similar to that of pelvic-floor tissue at the nanoscale/microscale. In addition, the mean pore size and porosity for microfibrous/microyarn scaffolds are shown in tables 1 and 2. They have an ideal range because larger pore size and higher porosity increases cell migration, nutrient flow and metabolite release [25].

To ensure transplantation in the body, electrospun scaffolds should provide appropriate mechanical strength. We mixed TPU with P(LLA-CL) with different weight ratios of P(LLA-CL) to TPU. Microyarn scaffolds showed slightly weaker mechanical properties than microfibrous scaffolds (figure 2, tables 1 and 2). However, there was no significant difference between microfibrous and microyarn scaffolds with regard to tensile strength and elongation. For microfibrous scaffolds, with decreasing blend ratios of P(LLA-CL) to TPU from 100 to 0, the mean tensile strength and mean elongation at the break increased significantly. However, for microyarn scaffolds, P(LLA-CL)/TPU at a weight ratio of 50:50 possessed higher tensile strength than the weight ratios of blended P(LLA-CL) to TPU at 0:100 and 25:75. This phenomenon may be associated with each part of the dynamic liquid electrospinning process, including the stability of eddy currents and hydrophilicity of polymers. In addition, the mechanical properties of electrospun blend microfibrous scaffolds were strongly affected by microfiber structure, the properties of each polymer in mixed microfibrous scaffolds and interaction between each polymer microfiber [26]. The core reason for such mechanical behavior merits further investigation.

According to Rubod *et al*, the maximum strength of human vaginal walls is 2.12 ± 0.1 MPa to 4.53 ± 0.18 MPa, and their maximum strain is 19 ± 2.03% to 41 ± 1.06% [27]. According to Calvo *et al*, the maximum strength of human vaginal walls is ≈8.40 MPa (figure 2; mean data for each patient [28]). Our results showed that the mechanical properties of the weight ratios of P(LLA-CL) to TPU microyarn scaffolds at a weight ratio of 50:50 exhibited better tensile strength and elongation at the break than native vaginal walls, suggesting that mechanical support and elasticity are suitable for damaged tissues of the pelvic floor. Moreover, compared with microfibrous scaffolds, microyarn scaffolds showed higher porosity, which is the basis for improving the adhesion and proliferation of cells (figures 2(*b*), (*d*) and (*e*)). Taking into account porosity, biodegradability, mechanical properties and biocompatibility, although these scaffolds could not

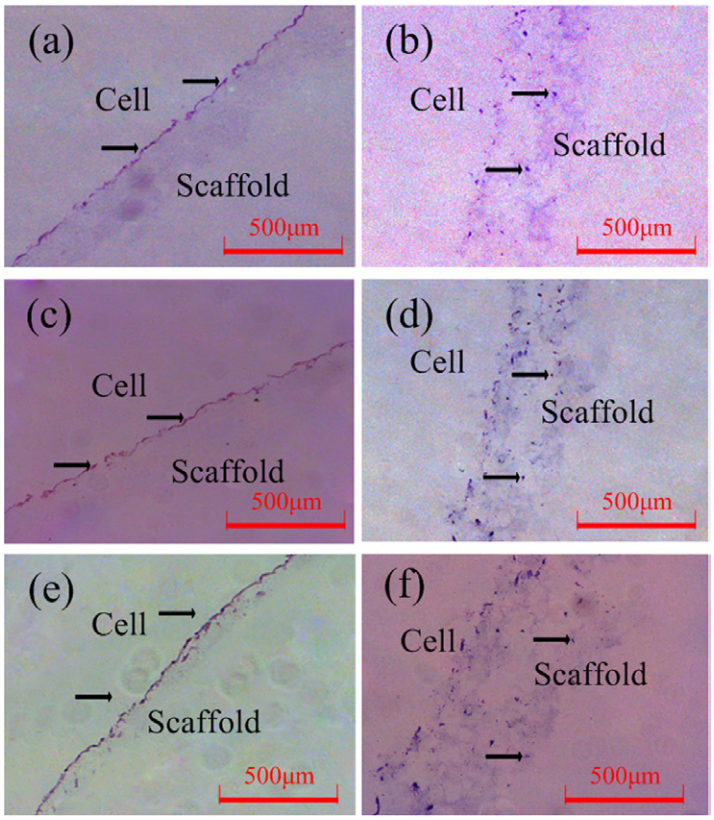


**Figure 8.** H & E-stained images show ADSC infiltration (black arrows) in microfibrous scaffolds (*a*), (*c*), (*e*) and microyarn scaffolds (*b*), (*d*), (*f*) at 1, 4 and 7 d, respectively. Scale bar = 500 $\mu$m.

match the flexibility and stiffness of native pelvic tissues, the weight ratios of P(LLA-CL) to TPU at 50:50 microyarn scaffolds were in accordance with the requirements of our study.

In this study, analyses of FTIR spectroscopy revealed that P(LLA-CL) and TPU had no obvious chemical reaction. Composite P(LLA-CL) and TPU scaffolds contain functional groups (e.g. carboxyl, hydroxyl, amino) that can improve the biocompatibility and hydrophilicity of such scaffolds [29].

SEM and CCK-8 assays revealed that ADSCs became attached and proliferated on the two types of scaffold. Most of the cells were still viable and few dead cells were detected on days 1, 4 and 7 (figures 5 and 7). This finding suggests that microyarn and microfibrous scaffolds were not cytotoxic. Also, blend microyarn scaffolds improved the adhesion and proliferation of cells compared with microfibrous scaffolds and tissue-culture polystyrene plates (TCPs). One reason for this phenomenon could be that microyarn scaffolds have higher porosity and larger pore size. Similar results have been reported by Xu *et al* for cultures of tendon cells on electrospun P(LLA-CL)/collagen microyarn scaffolds [30]. Furthermore, ADSCs attached to and grew well along microyarns and retained their normal shape, which extended to the internal structure of microyarn scaffolds (figures 5(*b*), (*d*) and (*f*)). These SEM micrographic observations suggested that the trend of ADSC proliferation could be quantified by CCK-8 assays. Hence, microyarn scaffolds could better support the proliferation of ADSCs compared with microfibrous scaffolds and the TCP culture system.

We studied the infiltration and growth of ADSCs through H&E staining (which demonstrated the relative depth of ingrowth within both types of scaffolds). ADSCs grew on the surface of conventional scaffolds even after 7 d, whereas cells on the microyarn scaffolds migrated gradually into the scaffolds. These results may have been due to the large pore size and porous structure, which facilitated cell migration into the scaffolds. Conversely, few cells grew on superficial conventional electrospun scaffolds due to their tightly packed structure. These data confirmed that microyarn scaffolds offered more suitable conditions for the attachment and infiltration of cells than conventional electrospun scaffolds.

## 5. Conclusion

To improve cell infiltration, we used novel dynamic liquid electrospinning technology to fabricate macroporous and high-porosity blended P(LLA-CL)/TPU microyarn scaffolds. H & E staining and CCK-8 assays demonstrated increased proliferation and infiltration of cells for P(LLA-CL)/TPU microyarn scaffolds compared with conventional P(LLA-CL)/TPU microfibrous scaffolds. SEM and inverted fluorescence microscopy showed macroporous and porous microyarn scaffolds. These scaffolds exhibited

ideal mechanical properties on par with female pelvic tissues. Our method offers novel electrospun technology with great potential in engineering female pelvic tissue that can overcome current problems facing conventional electrospinning. The major challenge for dynamic liquid electrospinning is how to achieve large-scale production under controlled conditions.

## Acknowledgments

This work was supported by the Research Fund of Science and Technology Commission of Shanghai Municipality (13DZ1941404).

## Funding Sources

The Research Fund of Science and Technology Commission of Shanghai Municipality (13DZ1941404).

## Conflicts of Interest

No.

## References

[1] Jarret M E 2010 *Pelvic Floor Dysfunction, in Anorectal and Colonic Diseases* (Berlin: Springer) pp 611–25
[2] Cervigni M and Natale F 2001 The use of synthetics in the treatment of pelvic organ prolapse *Curr. Opin. Urol.* **11** 429–35
[3] Baessler K and Maher C F 2006 Mesh augmentation during pelvic-floor reconstructive surgery: risks and benefits *Curr. Opin. Obstet. Gynecol.* **18** 560–6
[4] Amid P 1997 Classification of biomaterials and their related complications in abdominal wall hernia surgery *Hernia.* **1** 15–21
[5] Bako A and Dhar R 2009 Review of synthetic mesh-related complications in pelvic floor reconstructive surgery *Int. Urogynecol. J. Pelvic Floor Dysfunct.* **20** 103–11
[6] Haylen B T *et al* 2011 An International Urogynecological Association (IUGA)/International Continence Society (ICS) joint terminology and classification of the complications related directly to the insertion of prostheses (meshes, implants, tapes) and grafts in female pelvic floor surgery *Neurourol. Urodyn.* **30** 2–12
[7] Ridgeway B, Chen C C G and Paraiso M F R 2008 The use of synthetic mesh in pelvic reconstructive surgery *Clin. Obstet. Gynecol.* **51** 136–52
[8] Li W-J, Jiang Y J and Tuan R S 2006 Chondrocyte phenotype in engineered fibrous matrix is regulated by fiber size *Tissue Eng.* **12** 1775–85
[9] Blakeney B A, Tambralli A, Anderson J M, Andukuri A, Lim D J, Dean D R and Jun H W 2011 Cell infiltration and growth in a low density, uncompressed 3D electrospun nanofibrous scaffold *Biomaterials.* **32** 1583–90
[10] Van Tienen T G, Heijkants R G, Buma P, de Groot J H, Pennings A J and Veth R P 2002 Tissue ingrowth and degradation of two biodegradable porous polymers with different porosities and pore sizes *Biomaterials.* **23** 1731–8
[11] Baker B M, Gee A O, Metter R B, Nathan A S, Marklein R A, Burdick J A and Mauck R L 2008 The potential to improve cell infiltration in composite fiber-aligned electrospun scaffolds by the selective removal of sacrificial fibers *Biomaterials.* **29** 2348–58
[12] Ekaputra A K, Prestwich G D, Cool S M and Hutmacher D W 2008 Combining electrospun scaffolds with electrosprayed hydrogels leads to 3D cellularization of hybrid constructs *Biomacromolecules.* **9** 2097–103
[13] Baker S C, Atkin N, Gunning P A, Granville N, Wilson K, Wilson D and Southgate J 2006 Characterisation of electrospun polystyrene scaffolds for 3D *in vitro* biological studies *Biomaterials.* **27** 3136–46
[14] Beachley V and Wen X 2010 Polymer nanofibrous structures: fabrication, biofunctionalization, and cell interactions *Prog. Polym. Sci.* **35** 868–92
[15] Xu C, Inai R, Kotaki M and Ramakrishna S 2004 Electrospun nanofiber fabrication as synthetic extracellular matrix and its potential for vascular tissue engineering *Tissue Eng.* **10** 1160–8
[16] Pedicini A and Farris R J 2003 Mechanical behavior of electrospun polyurethane *Polymer* **44** 6857–62
[17] Tatai L, Moore T G, Adhikari R, Malherbe F, Jayasekara R, Griffiths I and Gunatillake P A 2007 Thermoplastic biodegradable polyurethanes: the effect of chain extender structure on properties and *in-vitro* degradation *Biomaterials.* **28** 5407–17
[18] Ma Z, Kotaki M, Yong T, He W and Ramakrishna S 2005 Surface engineering of electrospun polyethylene terephthalate (PET) nanofibers towards development of a new material for blood vessel engineering *Biomaterials.* **26** 2527–36
[19] Kingham P J, Kalbermatten D F, Mahay D, Armstrong S J, Wiberg M and Terenghi G 2007 Adipose-derived stem cells differentiate into a Schwann cell phenotype and promote neurite outgrowth *in vitro Exp. Neurol.* **207** 267–74
[20] Agrawal C and Ray R B 2001 Biodegradable polymeric scaffolds for musculoskeletal tissue engineering *J. Biomed. Mater. Res.* **55** 141–50
[21] Zeltinger J, Sherwood J K, Graham D A, Müeller R and Griffith L G 2001 Effect of pore size and void fraction on cellular adhesion, proliferation, and matrix deposition *Tissue Eng.* **7** 557–72
[22] Kwon I K, Kidoaki S and Matsuda T 2005 Electrospun nano- to microfiber fabrics made of biodegradable copolyesters: structural characteristics, mechanical properties and cell adhesion potential *Biomaterials.* **26** 3929–39
[23] Heydarkhan-Hagvall S, Schenke-Layland K, Dhanasopon A P, Rofail F, Smith H, Wu B M, Shemin R, Beygui R E and MacLellan W R 2008 3D electrospun ECM-based hybrid scaffolds for cardiovascular tissue engineering *Biomaterials.* **29** 2907–14
[24] Wu J, Liu S, He L, Wang H, He C, Fan C and Mo X 2012 Electrospun nanoyarn scaffold and its application in tissue engineering *Mater. Lett.* **89** 146–9
[25] Agrawal C M and Ray R B 2001 Biodegradable polymeric scaffolds for musculoskeletal tissue engineering *J. Biomed. Mater.* **55** 141–50
[26] Lee K H, Kim H Y, Ryu Y J, Kim K W and Choi S W 2003 Mechanical behavior of electrospun fiber mats of poly (vinyl chloride)/polyurethane polyblends *J. Polym. Sci. B: Polym. Phys.* **41** 1256–62
[27] Rubod C, Boukerrou M, Brieu M, Jean-Charles C, Dubois P and Cosson M 2008 Biomechanical properties of vaginal tissue: preliminary results *Int. Urogynecol. J. Pelvic Floor Dysfunct.* **19** 811–6
[28] Calvo B, Pena E, Martins P, Mascarenhas T, Doblare M, Natal Jorge R M and Ferreira A 2009 On modelling damage process in vaginal tissue *J. Biomech.* **42** 642–51
[29] Chandrasekaran A R, Venugopal J, Sundarrajan S and Ramakrishna S 2011 Fabrication of a nanofibrous scaffold with improved bioactivity for culture of human dermal fibroblasts for skin regeneration *Biomed. Mater.* **6** 015001
[30] Xu Y *et al* 2013 Fabrication of electrospun poly(L-lactide-co-epsilon-caprolactone)/collagen nanoyarn network as a novel, 3D, macroporous, aligned scaffold for tendon tissue engineering *Tissue Eng. C Methods.* **19** 925–36